Chapter 2
Water Waves in Isotropic and Anisotropic Media: A comparison

Check for updates

Leo R. M. Maas

Abstract Restoring forces as gravity, Coriolis force or their combination, endow geo and astrophysical fluids with an anisotropy direction. Breaking the underlying hydrostatic or cyclostrophic force balances in fluids that are stratified in density or angular momentum results in obliquely-propagating internal waves. These waves differ in nearly every conceivable aspect from external, surface gravity and capillary waves. Differences between linear internal and external waves stem to a large part from the complementary way in which their frequency depends on the wave vector. While these differences may be hiding in symmetrically-shaped basins, these become fully apparent when the boundary shape breaks the symmetry imposed by the anisotropy. These underlying force balances also constrain any wave-driven mean flows. Interestingly, the lack of a clear force balance in a homogeneous, non-rotating fluid that is stratified in linear momentum, renders waves, perturbations on these shear flows, 'problematic'.

2.1 Introduction

Waves in isotropic media, like familiar sound and electromagnetic waves in three-dimensional space, or gravity waves in the two-dimensional plane of the water surface, behave quite differently from waves in anisotropic media. Inside fluids, the directions of gravity and/or background rotation provide the fluid with an anisotropy which strongly influences wave propagation inside stratified and/or rotating fluids. Gravity, rotation and a nontrivial shape of the fluid domain are important ingredients in the fields of geophysical and astrophysical fluid dynamics. This warrants consideration of the specific consequences of these properties, and a comparison between isotropic external and anisotropic internal waves. The aim of this paper is to juxtapose well-known properties of isotropic surface water waves with those exhibited by anisotropic waves in stratified/rotating fluids.

L. R. M. Maas (✉)

Institute for Marine and Atmospheric Research (IMAU), Utrecht University, Utrecht, Netherlands
e-mail: L.R.M.Maas@uu.nl

In Sect. 2.2.1, we start by considering external waves: isotropic gravity waves propagating on the surface of homogeneous-density fluids. This deals with the specific nature of their dispersion relation, its implications for wave ray divergence and wave ray chaos, and the modifying influence of background rotation on long surface gravity waves. This leads to a brief discussion of Sverdrup, Poincaré and Kelvin waves (see also Chap. 4 of this book), as well as to amplitude and phase patterns displaying amphidromic points, phase-singularities where phase is multi-valued and vertical displacement vanishes.

Section 2.2.2 discusses two types of heterogeneous fluids that are density-stratified, supporting internal waves. The first type consists in layers of fluid that differ in density. Two-layer fluids allow for interfacial gravity waves that propagate horizontally along the average position of the interface, the pycnocline, which acts as a wave guide. These interfacial waves behave similar to surface waves because layers of uniform average depth inherit isotropy. The second type of internal gravity waves, found in continuously-stratified and particularly in uniformly-stratified fluids, obey another type of dispersion relation. Internal gravity waves propagate as beams, along paths that are inclined relative to the direction of gravity. A uniform water depth may again render the fluid superficially isotropic—up and downward propagating beams combine into vertically-standing, horizontally-propagating internal wave modes— but variations in water-depth reveal the true underlying anisotropic nature of stratified fluids. Upon reflection from sloping bottoms and side walls, internal wave beams lead to wave convergence and wave attractors.

Homogeneous-density fluids can still stratify, namely in linear momentum— known as shear flows—or in angular momentum, known as swirling flows. Both types of stratification support waves, although, as discussed in Sect. 2.3.1, those in the latter case are easier to observe. Solidly rotating fluids, for which the angular velocity is spatially uniform and constant, offer an important special case of swirling flows. When container motion produces this state the shear flow is deceptively simple. Upon passing through a viscous spin-up phase, observed from a co-rotating frame of reference, the flow recedes to a quiescent equilibrium state which obscures the underlying force balance. However, once this balance is perturbed it provides restoring Coriolis forces. Solid-body rotation invites a consideration of perturbations, called inertial waves, from within the co-rotating frame of reference, especially when the isotropy of the fluid domain is broken, discussed in Sect. 2.3.2.

The paper ends briefly discussing the effects of these waves on mean flows, Sect. 2.4, and gives some conclusions in the final Sect. 2.5.

2.2   Gravity Waves

Gravity waves arise both at free boundaries of fluid layers as external waves, as well as in their interiors as internal waves when the fluid is stratified in density. We discuss the far-reaching differences between these two types of waves, both with respect to their dispersion relations, reflection laws, as well as their regularity.

2.2.1 Surface Gravity Waves in Homogeneous Fluids

An inviscid, incompressible, non-rotating, quiescent uniform-density fluid does not
support any hydrodynamic waves unless its surface is free and subject to gravity or
capillary forces. These waves are external (boundary) waves as they propagate along
the boundary of the fluid body. They are surface-trapped as wave-induced motions
decay exponentially below the surface. These perturbations to the state of rest can
be described by the linearised Euler equations. When vorticity is initially absent, the
fluid will stay irrotational as vorticity is either created by friction at boundaries—a
viscous process—or by baroclinic torques, due to misalignment of density and pres-
sure gradients, excluded in a homogeneous-density fluid. Together with incompress-
ibility this guarantees that the waves can be described by a scalar velocity potential,
ϕ, that obeys a Laplace equation, $\nabla^2 \phi = 0$, where $\nabla^2 = \partial_{xx} + \partial_{yy} + \partial_{zz}$ denotes
the Laplacian operator. This elliptic equation, a sum of second-order spatial deriva-
tives, determines the spatial structure of the waves in a Cartesian (x, y, z) frame of
reference. Their temporal behaviour follows from boundary conditions describing
continuity of pressure across the surface, and by requiring fluid parcels that sit at the
surface to remain at the surface. Linear, constant-coefficient equations can be solved
by complex space-time exponentials. The physical content of a particular wave is
contained in its dispersion relation, $\omega(\mathbf{k})$, that describes how wave frequency, ω,
depends on wavevector $\mathbf{k}$'s magnitude and direction.

Wave Dispersion in Isotropic Media

As for plane monochromatic acoustic and electromagnetic waves in isotropic three-
dimensional space, gravity and capillary waves that propagate horizontally along the
free surface have frequencies that depend only on wave vector magnitude $\kappa \equiv |\mathbf{k}|$ (or
wavelength $\lambda = 2\pi/\kappa$), *not* on its direction. Restricting ourselves to gravity waves,
the vertical structure of these external waves varies from exponentially-decaying,
for short waves ($\kappa H \gg 1$), to vertically-uniform, for long waves ($\kappa H \ll 1$). Here
H denotes uniform fluid depth. In these regimes, frequency ω varies from $\omega = \sqrt{g\kappa}$
to $\omega = \sqrt{gH}\kappa$, and the waves change from dispersive to dispersionless respectively.
Here g denotes the acceleration of gravity. For any function, $\omega(\kappa)$, its restricted
dependence on the wave vector immediately implies the familiar property that a wave
group propagates its energy, related to that of its envelope, into the same direction
as its individual crests and troughs. Energy is transported with the group velocity
(the wave vector gradient of the wave frequency, $\mathbf{c}_g = \nabla_{\mathbf{k}}\omega = \mathbf{k}\,\kappa^{-1}\partial_\kappa\omega$), while
crests and troughs—two particular phases of the wave—propagate at phase velocity,
$\mathbf{c} = \omega\mathbf{k}/\kappa^2$, also pointing parallel to the wave vector $\mathbf{k}$. This alignment happens even
when, due to a nonlinear dependence of wave frequency on wave vector magnitude,
the waves constituting the group propagate at different speed, leading them to disperse
and the wave group to spread. This type of dispersion relation obviously provides
a constraint on the wavelength, which is fixed by the wave's frequency. Because of

this tight relationship between wave frequency and wavelength, in electromagnetism these are described by the single term 'color'.

Diverging External Waves and Wave Ray Chaos

Regardless of the horizontal shape of a container's vertical side-walls, a surface wave cannot change its frequency when it reflects. The amount of waves that will reflect off a wall is the same as the amount that are incident. The dependence of frequency on wave vector magnitude implies that the wavelength does not change either during reflection. Since the velocity vector produced by surface waves, $\mathbf{u} = \nabla\phi$, is given by the gradient of a velocity potential ϕ, it is parallel to the wave vector, $\mathbf{u} \parallel \mathbf{k}$. When waves are incident on a vertical wall, vanishing of the normal velocity component at the wall implies that normal wave vector components of incident and reflected waves have to match in magnitude while differing in sign. Together with the fact that wave vector magnitude cannot change during reflection this implies that the waves reflect specularly. This expresses the Snell-Descartes law, stating that a wave's angle of reflection relative to the wall's normal equals its angle of incidence.

While the presence of wave vector magnitude in the dispersion relation thus provides a constraint on the reflecting wave's length, the *absence* of the wave vector direction also has its significance: waves can adjust their propagation direction whenever there is reason to do so, for instance when they reflect from a curved vertical boundary. They will then scatter into multiple directions, at each point of the boundary reflecting specularly, see Fig. 2.1. This type of scattering reveals the natural tendency of surface gravity wave rays to diverge.

In an irregularly-shaped cavity, the unknown frequency of an arbitrarily located wave source can be extracted by measuring the wavelength (wave vector magnitude) over any part of the cavity. In an enclosed, but complex-shaped fluid basin, multiple reflections then give rise to 'wave ray chaos' (Berry 1981). Interestingly, surface waves still linger along a restricted set of periodic ray paths, where the rate of divergence is smallest. These paths stand out as 'scars': locations where those waves occur preferentially, see Fig. 2.2.

Rotational Modification of Long Surface Gravity Waves

When a homogeneous-density, free-surface fluid rotates, such as on Earth, the external waves—and especially the long, plane surface gravity waves—are modified. In a uniform-depth basin, rotating in an anticlockwise sense at rate Ω around an axis normal to the equilibrium surface, long waves are governed by the Rotating Shallow-Water Equations (RSWEs)

$$
\begin{aligned}
u_t - v &= -\zeta_x, \\
v_t + u &= -\zeta_y, \\
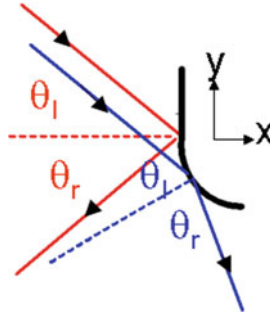\zeta_t + u_x + v_y &= 0.
\end{aligned}
\tag{2.1}
$$

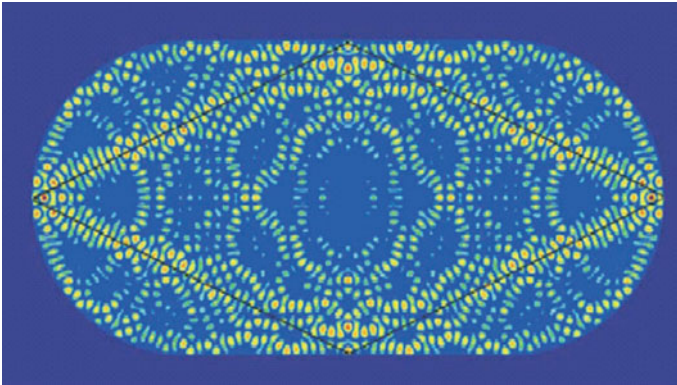**Fig. 2.1** Surface wave rays reflecting from curved vertical boundary

Fig. 2.2 Surface wave scars in a stadium showing large (yellow) and small (blue) amplitude disturbances. Solid lines show an unstable periodic orbit. Figure adapted from Heller (1984)

Here we use subscript-derivative notation and dimensionless variables. Time t is scaled with the Coriolis frequency $f = 2\Omega$. For convenience we take its expression as relevant in a laboratory model, instead of its geophysically-motivated expression $2\Omega \sin \varphi$ which in the traditional approximation would apply at latitude φ on a plane tangent to the Earth (Gerkema et al. 2008). The vertical, z, and surface elevation, ζ, are scaled with depth, H, horizontal (x, y)-coordinates with Rossby deformation radius, $R \equiv \sqrt{gH}/f$, and velocities, (u, v), with, $Rf = \sqrt{gH}$. As is well-known (see e.g. Gill (1982)), depending on geometric constraints, system rotation gives rise to Sverdrup, Poincaré and Kelvin waves (see Chap. 4 of this book). Over a uniform-depth sea, plane monochromatic Sverdrup waves $\propto e^{i(kx+ly-\omega t)}$ obey the dispersion relation

Fig. 2.3 Surface elevation ζ (solid and dashed for positive or negative displacements) for a Poincaré wave (sum of two Sverdrup waves) propagating in a channel into a direction indicated by the red arrow. Notice that nodal lines are displaced from the middle axis towards the coast that is on the right hand side, as seen from its propagation direction
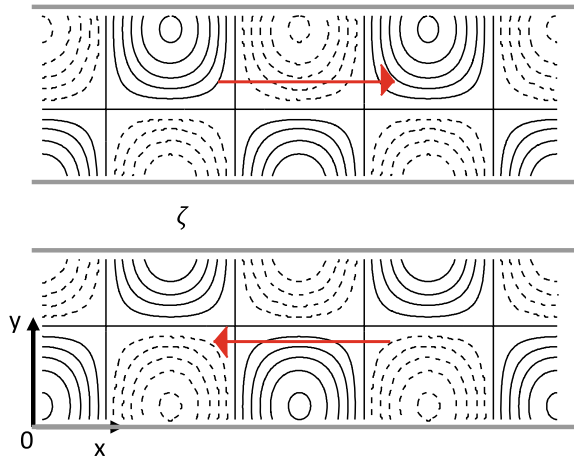
$$\omega^2 = 1 + k^2 + l^2 = 1 + \kappa^2, \tag{2.2}$$

where $\mathbf{k} = (k, l) = \kappa(\cos\phi, \sin\phi)$, for waves propagating in direction ϕ relative to a pre-chosen orientation of the x-axis. The first term on the right-hand side represents the dimensionless Coriolis frequency, acting as low-frequency cut-off. Sverdrup waves occur on the infinite plane (Sverdrup 1926) and (2.1a,b) imply that system rotation induces elliptically-polarized currents. The presence of a vertical wall, at $y = 0$ say, requires a combination of incident and reflected Sverdrup waves—a Poincaré wave—to satisfy the impermeability condition, $\mathbf{u} \cdot \mathbf{n} = v = 0$, see Fig. 2.3 where $\mathbf{n}$ denotes a unit vector normal to the boundary directed outwards.

Kelvin waves, also propagating along one such a wall, simplify the dispersion relation to $\omega = k$, by having its transverse wavenumber $l = i$. In that case a low-frequency cut-off is absent. In order that the wave decays away from the wall as $y \to \infty$, only the positive sign of $\sqrt{k^2}$ is allowed. This implies propagation in positive x-direction. Regardless of wave frequency, this transverse decay occurs dimensionally always at the Rossby deformation scale, R.

External waves, such as short gravity waves, decaying exponentially below the surface, can be interpreted as a boundary wave whose dimension is reduced by one. Two-dimensionality of these waves is captured by integrating over the (vertical) decay direction. As horizontal currents associated with long waves are independent of the vertical coordinate, this decay is no longer visible. It occurs over a scale depth much larger than the fluid depth. Formally, these waves still present a dimensionally-reduced (surface trapped) wave feature. This can be treated as such by vertically integrating the equations. In the same vein, a Kelvin wave provides a further dimensional reduction, owing to its additional exponential decay, transverse to the coast. Integrating also over the direction perpendicular to the coast it can be described as a one-dimensional wave feature.

Amphidromic Wave Systems

In partially, or fully-enclosed rotating water bodies, such as inland seas and lakes, impermeability of its side walls requires a combination of Kelvin and Poincaré waves (see Chap. 4 of this book). This gives rise to intricate structures called *amphidromes*, see Fig. 2.4. Amphidromes are phase-singularities (points where phase is multi-valued) that coincide with nodal points: locations of zero elevation amplitude. Attempting to understand the spatial pattern of simultaneously observed tidal displacements along the North Sea's perimeter, Whewell (1833) inferred the presence of such points. He postulated their existence in an attempt to construct tidal co-phase lines—lines connecting points simultaneously reaching for instance high or low water. Solutions of the RSWEs also display 'spider-web like' structures, as found in (semi) rectangular and square basins of uniform depth (Proudman 1916; Taylor 1922; Rao 1966), and more recently in basins of variable bottom depth and boundary shape (Steinmoeller et al. 2019). These arise because rotationally-modified surface gravity waves need to satisfy an impermeability condition at boundaries. When cast in terms of the free surface elevation, ζ, this takes the form of an oblique-derivative (Robin) boundary condition, a weighted combination of Dirichlet and Neumann boundary conditions. Amphidromes already appear in straight, open channels, where they form due to two counter-propagating Kelvin waves, see Fig. 2.5 (Krauss 1973). Section 2.3.2 will discuss replicas of such structures in the interior inertial wave field, interestingly arising in fully confined (rigid-lid), homogeneous-density rotating fluids.

Fig. 2.4 Amplitude (dashed, arbitrary units) and phase lines (solid, each 30 °C) of the surface elevation for the computationally determined lowest frequency, rotationally-modified surface gravity wave in a rotating square basin. It displays a cyclonic amphidromic point in the centre where the amplitude vanishes and phase is multi-valued. Figure from Rao (1966)
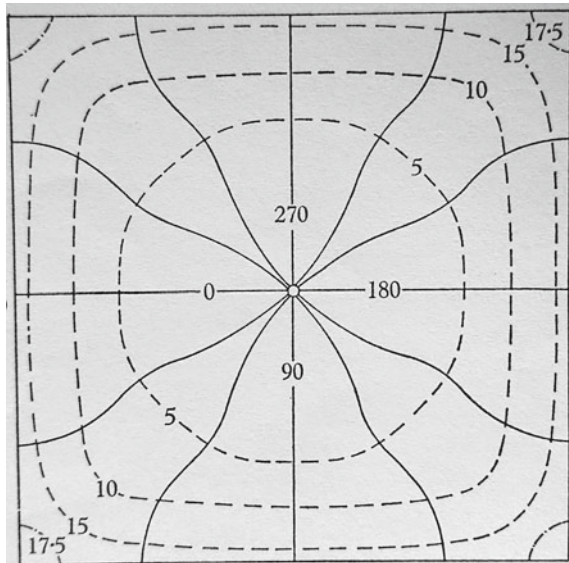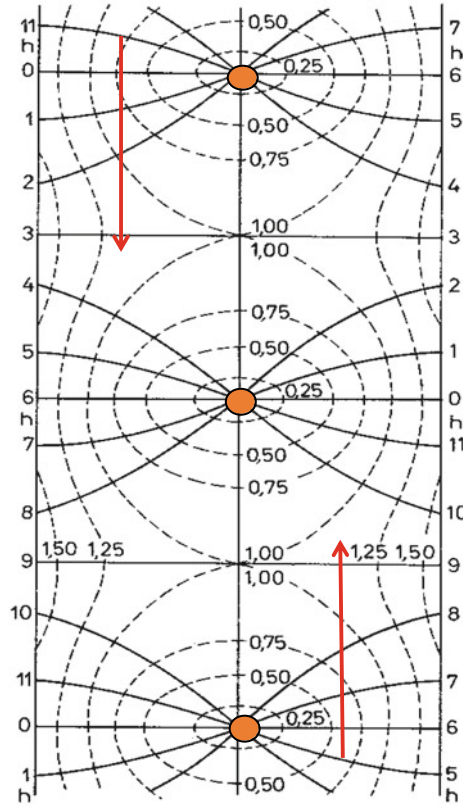
Fig. 2.5 Amplitude lines (dashed, arbitrary units) and phase lines (solid, each 30 °C) of the sea surface elevation produced by two counter-propagating Kelvin waves (propagation direction indicated by red arrows) of equal amplitude displaying amphidromic points (orange dots) where the amplitude vanishes and phase is multi-valued

2.2.2 Gravity Waves in Heterogeneous Media

Interfacial Waves

In the foregoing we interpreted surface waves in isotropic fluids as external or boundary waves. Alternatively, an external or boundary wave can be defined as a wave whose maximum displacement (in vertical or horizontal direction) occurs at the bounding surface. According to this definition, waves that have their maximum displacements below the free surface should be interpreted as internal waves. From that perspective, the waves that Franklin (1762) discovered at the interface between oil and water—two immiscible fluids of different density—might well be interpreted as internal waves, as their maximum displacements occur in the interior of the fluid. However, we refrain from this interpretation as waves still decay exponentially, below as well as above the interface. In that sense, these interfacial waves belong to the class of boundary waves, being external to the two fluid bodies of homogeneous-density that make up the two-layer fluid. Indeed, waves propagating at the interface between two fluid layers of different density but uniform depths are very akin to surface waves.

Apart from an additional, fluid-gas phase-transition, the free surface again separates two liquids differing in density (albeit by a factor thousand bigger than that between oil and water). Consequently, the dispersion relation satisfied by interfacial waves is very similar to that of surface waves. In particular, the frequency is again independent of wave vector direction, merely leading to a reduction of the acceleration of gravity by a factor equalling the ratio of the density difference between the two layers to their average density (Stokes 1847).

Two-layer stratification form one *end member* of the general class of density-stratified fluids. These are quite common in natural conditions, and occur for miscible fluids too. In shallow seas they form due to a combination of wind and tidal mixing that stir warm surface and cold bottom layers respectively, leaving a density jump at an interface in between. They also frequently occur near fjords, when fresh melt water spreads out over salty ocean water. It is in the latter situation that the existence and relevance of interfacial waves was first brought to light in an oceanographic context. These waves helped demystify the *dead-water* phenomenon encountered by Nansen at the end of the nineteenth century. Dead-water pertains to a sudden, sharp drop of a boat's speed when traversing a fjord (Nansen 1902). This loss of propulsion appears to occur when a boat's hull moves in the vicinity of an interface between low density fresh and high density salt fluid layers. When its velocity matches the interfacial wave speed it generates interfacial waves, leading the boat to suffer from excessive interfacial wave drag (Ekman 1904).

Wave Modes Versus Beams in Heterogeneous Fluids

Theoreticians also considered waves in three-layer, multi-layer, continuous and uniform stratifications (Rayleigh 1883; Burnside 1888; Love 1890). For internal gravity wave history, see the excellent review of Hinwood (1972). These waves are perturbations of a *hydrostatic equilibrium*,

$$(\rho_* + \rho(z))g = -\frac{dp}{dz},$$ (2.3)

in which the downward-directed force of gravity, acting on fluid of local density consisting of a large constant ρ_* and a small depth-varying $\rho_0(z)$ part, balances the upward-directed pressure gradient force. This leads to a hybrid ensemble of boundary waves, propagating along interfaces, as well as, in the continuously-stratified fluid, to what could be called 'genuine internal waves'. The latter waves have their maximum displacements in the fluid interior and are not trapped to any particular interface. Initially, it was held expedient to assume the bottom to be parallel to the free surface, and consider a uniform-depth fluid. The benefit of this was that separation of variables was still possible, such that horizontally-propagating internal waves have a matching vertical structure. Approximating the surface as rigid, by requiring the vertical velocity to vanish at surface and bottom, the vertical modes are quantized by the finite depth. Indeed, this assumption on basin geometry and consequent

separability allowed for the computation of vertical modal solutions, even when the stratification was continuous yet non-uniform (Fjeldstad 1933; Groen 1948).

At the expense of a more fundamental, plane internal wave approach, that takes the form of an obliquely-propagating internal wave *beam*, this 'modal approach' subsequently dominated the interpretation and understanding of internal wave behaviour in the ocean. To be sure, the modal and beam approaches are reconcilable in uniform-depth, uniformly-stratified fluids, in which stability frequency $N(z)$ is assumed constant, a second *end-member* type of stratification. In Boussinesq approximation, the square of the stability frequency, $N^2 \equiv -g\rho_*^{-1}d\rho_0(z)/dz$, relates to the background density gradient. The beam's inclined orientation relative to gravity betrays that genuine internal waves propagate under a particular, fixed angle α, determined by the dispersion relation that perturbations satisfy:

$$\omega/N = \pm \cos\alpha. \tag{2.4}$$

In this case, angle α measures the direction of phase and group velocity vectors with respect to the horizontal and vertical, respectively. Assume the wave vector lies in the vertical (x,z)–plane in which the wave propagates, $\mathbf{k} = (k, 0, m) = \kappa(\cos\alpha, 0, \sin\alpha)$, then $\mathbf{c} = \omega\mathbf{k}/\kappa^2 = \omega\kappa^{-2}(k, 0, m) = \pm N \cos^2\alpha\kappa^{-1}(1, 0, \tan\alpha)$ (phase velocity) is perpendicular to group velocity vector $\mathbf{c_g} = \nabla_\mathbf{k}\omega = \partial_\alpha\omega\,\nabla_\mathbf{k}\alpha$, which evaluates to $\mathbf{c_g} = \pm N \sin\alpha\kappa^{-2}(m, 0, -k) = \pm N \sin^2\alpha\kappa^{-1}(1, 0, -\cot\alpha)$, although both share the same horizontal propagation direction.

The internal wave dispersion relation (2.4) betrays that a uniformly-stratified fluid is *transparent* to internal waves. 'Transparency' means that wave scattering occurs only at the boundary. Transparency can be maintained for some special non-uniform stratifications (Grimshaw et al. 2010). But to a good approximation it holds whenever the length scale over which the density gradient varies is large compared to the wavelength of the internal wave, so that $N = N(\varepsilon z)$, where ε denotes a small parameter and a WKB-approximation applies. For this situation, the inclination of a fixed-frequency ($\omega = constant$) wave can be obtained by a local application of the dispersion relation (2.4) and depth variations in amplitude and beam-inclination occur *adiabatically*, without any partial reflection or trapping inside the fluid (Hazewinkel et al. 2010b). This allows the vertical z-coordinate to be stretched, such that the equation describing the internal wave's spatial structure takes its canonical, hyperbolic form

$$\psi_{xx} - \psi_{zz} = 0. \tag{2.5}$$

Streamfunction $\psi(x, z)$ is introduced by virtue of two-dimensional incompressibility. Upon stretching the vertical, internal waves follow straight, inclined ray paths again. By contrast, when the density gradient varies rapidly, internal waves might also scatter inside the fluid on variations in the density gradient.

Internal Gravity Waves in Uniformly-Stratified Fluids

Adhering to the uniformly-stratified fluid in a basin of uniform depth, up and downward propagating beams of equal amplitude acquire a standing, sinusoidal vertical structure. Together with a complex exponential dependence on horizontal coordinate and time, these can obviously be interpreted as vertically-standing, horizontally-propagating modes. They present a seemingly straightforward extension of an interfacial wave. This interpretation however meets its limitations. It acquires horizontal, isotropic features due to depth-uniformity, which is lost in any real geophysical setting where depth variations scatter the incident beam.

Since an internal wave reflecting from a sloping bottom or side wall preserves its frequency, the dispersion relation implies that in this case the wave cannot change its wave vector inclination. This leads to anomalous, non-specular reflection. A single-frequency set of collinear waves differing in wave number magnitude and amplitude, defines an incident, compact wave beam of particular fixed inclination. This beam has a transverse width that will necessarily change when subject to *(de)focusing* reflections at an inclined boundary. Thus, depth-changes lead to a change of the wavelengths and amplitudes of the waves constituting the beam, see Fig. 2.6a. This precludes the persistence of a vertically-standing structure, built by beams of equal amplitude propagating in opposite vertical directions.

Converging Internal Waves and Wave Attractors

The ultimate fate of internal waves, generated by an oscillating cylinder, may not have been evident in the experiment shown in Fig. 2.6a. In confined basins, the focusing which internal wave beams experience upon bouncing at its boundaries, dominates
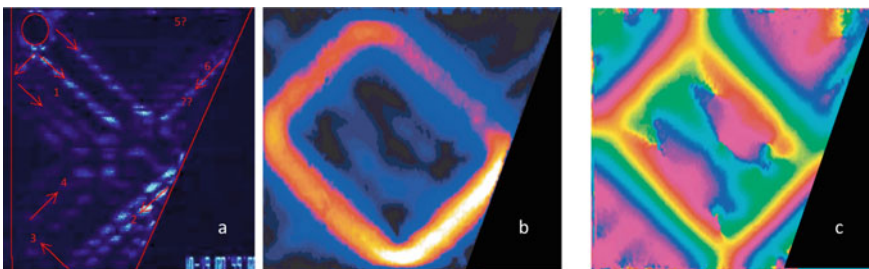

Fig. 2.6 Vertical transect of a uniformly-stratified fluid showing internal waves generated (**a**) by vertically-oscillating horizontal cylinder, located in the upper left (red circle) and **b**, **c** in a horizontally oscillating tank. The trapezoidal basin has rigid walls, both along the sloping and vertical side walls, as well as at top and bottom. (a) Arrows indicate the internal wave energy propagation direction. Successively reflected internal wave beams are numbered in sequential order. Courtesy of Frans-Peter Lam. **b** Amplitude (black: zero, white: most intense) and **c** phase (cyclic colors), adapted from Hazewinkel et al. (2010b)

over defocusing, leading to the formation of wave attractors, see Figs. 2.6b, c and 2.7a. Incident, focusing wave beams have larger scattering cross-sections than the reflected beams and *vice versa* for defocusing waves. Here the scattering cross-section refers to the width of the beam perpendicular to the energy propagation direction. The two are equal only for reflections from horizontal or vertical boundaries, which are parallel or perpendicular to the anisotropy direction. In that case the beam-width does not change upon reflection. Exceptionally, a net change of beam-width is also absent for special, nontrivially-shaped basins, when focusing of waves of particular frequencies (hence propagation angles) during some boundary reflections is exactly balanced by defocusing during other reflections. As a consequence, such basins possess a denumerable set of globally-resonant modes, see Fig. 2.7b. The latter property, exhibited for instance by trapezoidal domains, relies on the existence of residual symmetries (Maas and Lam 1995).

These situations can be interpreted geometrically by following individual characteristics (internal wave rays). Launching a ray from an arbitrarily located boundary point, upon reflection at any of the boundaries it will retain its inclination to the vertical. For these exceptional geometries and frequencies, after a number of reflections each ray path returns to its launching position and becomes part of a periodic orbit of finite length, forming a globally-resonant mode, see Fig. 2.7b. However, for all other frequencies in these basins—frequencies filling non-denumerable, continuous
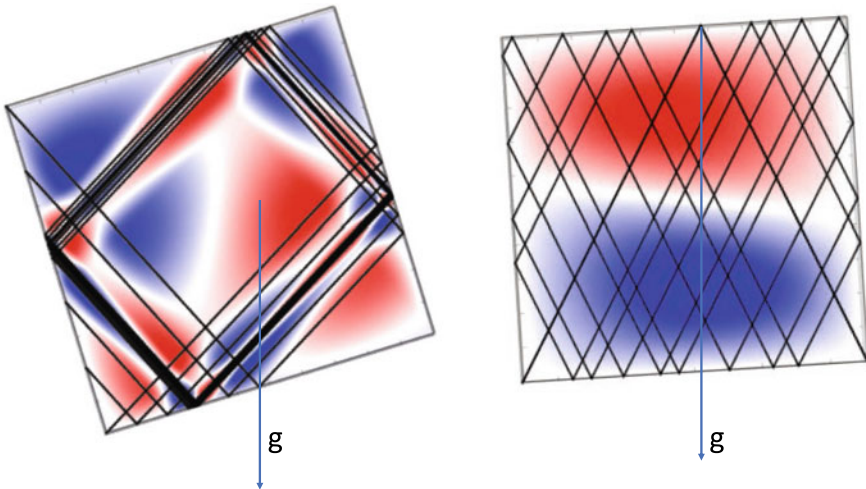

Fig. 2.7 Side view of internal gravity waves of two different frequencies in a uniformly-stratified fluid in a tilted square basin. Individual characteristics (lines) with which streamfunction field (color) is geometrically constructed (Maas and Lam 1995) retain their inclination relative to gravity, **g**, whose direction is indicated by an arrow. The generic response for arbitrary frequencies is given by wave attractors (left) and exhibits focusing of characteristics onto an attractor; the globally resonant modes (right) are exceptional, relying on periodicity of underlying individual characteristics. Courtesy of Stefan Kopecz

frequency bands—rays are non-periodic and infinitely long. Only a denumerable set of finite-length periodic orbits remains. These orbits attract all non-periodic orbits, see Fig. 2.7a where only one such attracting orbit exists.

For basins of generic shape that lack this residual symmetry, such as a parabolic basin, the basin shape breaks this residual symmetry too. There will be no exceptional frequencies, so no globally-resonant modes. Only a few periodic orbits remain, that attract all waves of a particular frequency. These limit cycles, *wave attractors*, are reached regardless of the wave's source location.

2.3 Inertial Waves

We will consider the implications of wave attractors later on, after taking a look at waves supported by shear flows, with, as important special case, the waves in swirling flows, and especially those in a solidly-rotating fluid. Owing to the anisotropy produced by rotation, combined with a symmetry-breaking basin shape, inertial waves supported by homogeneous-density, rotating fluids also show the presence of wave attractors.

2.3.1 Waves in Shear Flows

Homogeneous-density shear flows, $\mathbf{u} = (u, v, w) = (U(z), 0, 0)$, support waves which are stable manifestations of shear-flow perturbations. These form the complement of the much wider studied class of shear-flow instabilities (Drazin and Reid 1998; Carpenter et al. 2011). Since Squire's theorem asserts that two-dimensional perturbations turn unstable before three-dimensional disturbances do (Squire 1933) we consider two-dimensional, monochromatic plane wave perturbations $\propto e^{ik(x-ct)}$, governed by

$$
\begin{aligned}
ik(U - c)u + wU' + ikp &= 0, \\
ik(U - c)w + p' &= 0, \\
iku + w' &= 0,
\end{aligned}
\tag{2.6}
$$

where a prime denotes a z-derivative. We describe these perturbations on a shear flow in terms of a streamfunction, $\psi = \Psi(z)e^{ik(x-ct)}$, that vanishes at the bottom and surface, $z = z_{1,2}$. Inserting perturbation velocities in these equations, $u = \partial\psi/\partial z$, $w = -\partial\psi/\partial x = -ik\psi$, yields Rayleigh's stability equation (Rayleigh 1879)

$$
(U - c)\left(\frac{\partial^2 \Psi}{\partial z^2} - k^2 \Psi\right) - U'' \Psi = 0.
\tag{2.7}
$$

Infer the stability of the shear flow by assuming that the frequency and thus phase speed is complex, $c = c_r + ic_i$. The presence of a non-zero imaginary part, c_i, signals

instability. Dividing (2.7) by $U - c$, multiplying by the complex-conjugate, Ψ^*, integrating between bottom and (rigid) surface (using integration by parts for the first term) and separating the real and imaginary parts, the latter is given by

$$c_i \int\limits_{z_1}^{z_2} \frac{U''}{|U - c|^2} |\Psi|^2 \, dz = 0.$$

Parallel shear flows are stable ($c_i = 0$) when its background vorticity gradient U'' does not switch sign within the channel (Rayleigh's stability criterion). We will see an example shortly.

Waves in a Linear Shear Flow

A simple type of shear flow, a Couette flow, $U(z) = z$, lacking any curvature, $U'' = 0$, also supports waves propagating down a channel, $-1 \leq z \leq 1$, provided at some depth within the channel, z_c, the phase speed matches the background flow, $c = U(z_c)$: a critical layer. In this case, (2.7) is written (Drazin and Reid 1998)

$$\frac{\partial^2 \Psi}{\partial z^2} - k^2 \Psi = \delta(z - c), \tag{2.8}$$

allowing for exponentially-decaying waves on either side of the critical depth, $z_c = c$, and appropriately vanishing at the boundaries

$$\begin{aligned} \Psi(z) \propto \sinh k(c - 1) \sinh k(z + 1), \ -1 \leq z \leq c \\ \sinh k(c + 1) \sinh k(z - 1), \ c \leq z \leq 1. \end{aligned} \tag{2.9}$$

For any horizontal wave number, k, and any phase speed $|c| < 1$, this admits a continuous spectrum of waves, all trapped to their respective critical-depth. In a sense these all again belong to the class of isotropic boundary waves, as they decay exponentially away from the critical layer and do not propagate into the transverse z-direction.

For shear flows possessing curvature, a similar type of external wave exists at depth z_s where the shear flow has an inflection point, $U''(z_s) = 0$. Waves that propagate at a speed matching the local velocity at that depth, $U(z_s) = c$, can again be trapped at the critical layer $z = z_s$. But, in addition to waves belonging to the continuous spectrum, a discrete set of vertically-standing waves exists as we will see in the next subsection.

Waves in a Sinusoidal Shear Flow

Consider for example waves on a sinusoidal shear flow, $U = \sin z$, in a channel bounded by lines $z = z_{1,2}$, having, $z_1 \leq 0 \leq z_2$. This flow has an inflection point at $z = z_s = 0$. Then, for $c = 0$, its second derivative matches the prefactor of the first term in (2.7), and this equation factors into

$$\sin z \left(\frac{\partial^2 \Psi}{\partial z^2} + (1 - k^2)\Psi \right) = 0. \tag{2.10}$$

With the boundary conditions

$$\Psi = 0 \text{ at } z = z_1, z_2, \tag{2.11}$$

this equation has solutions

$$\Psi_s = \sin \left(n\pi \frac{z - z_1}{z_2 - z_1} \right), \quad k = \sqrt{1 - \frac{n^2 \pi^2}{(z_2 - z_1)^2}}, \tag{2.12}$$

which are unstable, growing spatially (k imaginary) for integer $n > (z_2 - z_1)/\pi$. This shows that a finite number of neutral (wave) modes exist when $z_2 - z_1 > \pi$. This provides a counter-example to Rayleigh's criterion, showing that the presence of an inflection point is a necessary but not sufficient condition for all modes being unstable (Drazin and Howard 1962).

A channel lacking inflection points, $U''(z) \neq 0$, $z_1 \leq z \leq z_2$, is thus neutrally stable (i.e. c has zero imaginary part). It therefore still supports a discrete spectrum of neutral waves when $U(z)$ is concave and $U''/(U - c) < -k^2 < 0$. Concavity means that for any z in any part (z_-, z_+) of the fluid domain, where $z_1 \leq z_- \leq z \leq z_+ \leq z_2$, the average of the velocities at the end points of this interval is less than the velocity at any intermediate position, $|(U(z_+) + U(z_-))/2| < |U(z)|$. In a frame of reference moving with the waves, around the location where the phase speed matches the mean flow, the combined shear flow and waves manifest themselves in the form of Kelvin's 'cat-eye' flow pattern.

In these considerations, the effects of viscosity have sofar been left aside, the reason being that intuition would assign to viscosity an additional ability to stabilize wave motions. However, the contrary was proven to be true. As Darrigol (2005) recalls, Prandtl suspected that viscous stresses may induce a phase difference between wall-parallel and wall-transverse velocity components. In that case, energy, conveyed by the unperturbed mean flow U to the waves through Reynolds stress acting on mean-flow shear, might exceed viscous damping, leading to their instability and growth. This renders experimental study of stable waves on shear flows difficult if not impossible. Attention has thus shifted to the nonlinear regime, where large-amplitude waves may coexist with turbulence (Sun et al. 2015)), often in the form

of a self–sustained interaction of shear-flow perturbations with stream wise rolls (Waleffe 1997).

The geometry of the fluid basin receives little attention in these studies. In two-dimensional (x, z) settings, the shear flow $U(z)$ is compatible only with a uniform-depth channel having its boundaries at $z_{1,2} = constant$. But a consideration of geometry becomes pertinent when discussing waves on shear flows in three-dimensional domains, for which the *transverse* channel shape, $z = h(y)$, may become important. We will discuss the relevance of transverse topography in the context of axisymmetric shear flows in the next section.

Waves in Swirling Flows

In a *non-rotating*, cylindrical (r, θ, z) frame of reference, a special type of shear flow develops: a swirling flow. This is characterized by an axisymmetric, azimuthal flow of arbitrary radial dependence, $u_\theta = V(r)$, which is in *cyclostrophic balance*:

$$-\rho \frac{V^2}{r} = -\frac{dp}{dr}. \qquad (2.13)$$

The outward directed centrifugal force is balanced by an inward directed pressure gradient force. Axisymmetric, monochromatic perturbations of this radially-dependent azimuthal flow allow for the introduction of a Stokes streamfunction, $\psi(r, z, t)$, as incompressibility implies that radial and vertical velocities can be obtained from $ru = \partial\psi/\partial z$, $rw = -\partial\psi/\partial r$. At this point the underlying cyclostrophic equilibrium state, (2.13), is lost out of sight, not only because the perturbation pressure is described by differences between the actual and the cyclostrophic pressure, but also because this perturbation pressure itself has been eliminated when deriving a vorticity equation by cross-differentiation and subtraction of the horizontal momentum equations. However, its importance will be stressed in Sect. 2.4.3, when discussing the implications that waves may have for mean flows.

The streamfunction's spatial part, $\psi = \Psi(r, z)e^{-i\omega t}$, is governed by

$$r \frac{\partial}{\partial r} \left(\frac{1}{r} \frac{\partial}{\partial r} \right) \Psi - \left(4\frac{\Omega_l^2}{\omega^2} - 1 \right) \frac{\partial^2 \Psi}{\partial z^2} = 0, \qquad (2.14)$$

where Rayleigh's discriminant,

$$4\Omega_l^2(r) \equiv \frac{1}{r^3} \frac{dA^2}{dr} = 2\frac{V}{r} \left(\frac{V}{r} + \frac{dV}{dr} \right), \qquad (2.15)$$

is, unconventionally, expressed as the square of the *local* Coriolis frequency, $2\Omega_l(r)$. This is twice the local rotation rate, Ω_l, that reduces to the constant rotation rate, Ω, in the case of solid-body rotation, $V = \Omega r$. Rayleigh's stability criterion, $\Omega_l^2(r) \geq 0$ for all r, implies that the square of the angular momentum, $A \equiv rV(r)$, must increase

monotonically with increasing radius (Rayleigh 1917). The square on A in (2.15) indicates that this criterion is insensitive to the direction of background rotation. For waves of frequency $|\omega| < 2|\Omega_l|$, the governing Eq. (2.14) has a negative sign in front of the last second-order derivative, which makes it a hyperbolic equation. This implies it supports a type of internal wave, called inertial or gyroscopic wave, discussed further in the next section. Inertial waves are, for example, observed in the swirling flow of liquid metal, when driven by a rotating and alternating electromagnetic field (Vogt et al. 2014).

In general, the r-dependence of the Rayleigh-discriminant implies these inertial waves are subject to scattering, trapping and tunnelling. The explicit, curvature-related radial dependence of the first term of (2.14) leads to additional amplitude variations. But an axisymmetric basin of maximum radius a and arbitrary axisymmetric depth profile $h(r)$ supports a cylindrically-rotating shear flow, described by

$$V = \sigma \frac{r^2}{a}. \tag{2.16}$$

This has local rotation rate

$$\Omega_l = \frac{\sqrt{6}\sigma}{2} \frac{r}{a} \tag{2.17}$$

and is transparent to low-frequency waves if $\omega \ll \sqrt{6}\sigma$. Transformed dimensionless radial, $s = r^2/2a^2$, and (stretched) vertical, $Z = z/H$, coordinates absorb the amplitude-decrease due to radial spreading. Here

$$H = \frac{a\sqrt{6}\sigma}{\omega}.$$

This transforms (2.14) into the canonical equation governing the spatial structure of monochromatic internal waves

$$\frac{\partial^2 \Psi}{\partial s^2} - \frac{\partial^2 \Psi}{\partial Z^2} = 0. \tag{2.18}$$

In basins of arbitrary radial shape, the method of characteristics can solve this equation (Maas and Lam 1995). It is prone to develop wave attractors for nearly all boundary shapes, $Z = h(s)/H$.

2.3.2 Waves in Rotating Basins

To describe perturbations, azimuthal flows $V(r)$ that possess arbitrary radial dependency do not favour any particular rotating coordinate frame over the inertial frame. However, when the flow is in solid-body rotation, $\Omega = constant$, and the azimuthal flow increases linearly with radius, $V = \Omega r$, it makes sense to use a frame of ref-

erence co-rotating with the flow. A transformed time-derivative then absorbs the advective terms and, as mentioned before, the Rayleigh discriminant becomes constant, $4\Omega_l^2 = 4\Omega^2$. In a cylindrical domain, this leads to separability of (2.14). A sinusoidal vertical dependency of Ψ splits-off from its radial, Bessel function dependence (Kelvin 1880). Requiring regularity at the origin, vanishing of Ψ at the cylinder boundaries, and periodicity in the azimuthal direction, together with impermeability constraints at top and bottom boundary, leads to a triple quantisation of these radial-azimuthal-vertical modes.

Intermezzo: Viscous Effects

When an axisymmetric, closed cylindrical domain is put into steady rotation, a solid-body rotating state is reached from the initial state of rest through a spin-up process. In axisymmetric basins this involves viscous Ekman boundary layers that transport momentum to the inviscid interior by means of a meridional circulation (Greenspan and Howard 1963; Weidman 1976). In non-axisymmetric basins, such as an *eccentrically*-positioned cylinder, or a basin of different shape, the fluid needs to respond 'instantaneously' when set into rotation. This is caused by a pressure torque which, in the incompressible description, transmits at once throughout the fluid domain. This is an approximation employed when pressure waves, propagating at the speed of sound, are much faster than any of the velocities involved. In this type of basin, the fluid's initial response is governed by vorticity conservation. The fluid aims to retain its initial state of zero absolute vorticity (Van Heijst 1989; Van Heijst et al. 1990)), so that, in the frame co-rotating with the container, it is initially described by a vortex having uniform anticyclonic vorticity. At later stages the flow is subject to viscous adjustment, due to friction at side-walls, bottom and top, occurring at the Ekman time scale, $E^{-1/2}\Omega^{-1}$, where Ekman number $E \equiv \nu/L^2\Omega \ll 1$ is defined in terms of kinematic molecular viscosity, ν, length scale, L, and time scale Ω^{-1}. During this phase, cyclonic vorticity develops. When the depth of the fluid is constant these processes lead to an arrangement of nearly circular cyclonic and anticyclonic cells that gradually decay on the still longer, diffusive timescale $E^{-1}\Omega^{-1} = L^2/\nu$. When the container depth varies, however, these cells keep on moving in an irregular fashion, and Ekman spin–up seems to be faster in the shallower parts of the fluid domain (Van Heijst et al. 1994; Li et al. 2012).

Linearized Rotating Euler Equations

For any boundary shape of a rotating container, $y = y_b(x)$, and for any location of the container relative to the rotation axis, solid-body rotation can be achieved (Van Heijst et al. 1994; Li et al. 2012). Viewed from the rotating, axial frame of reference, after spin-up, the fluid is in an apparent state of rest. In this steadily-rotating state, when fluid and bounding container move as a solid body, the effects of rotation and viscosity may no longer be visible. Yet, at any point within the fluid domain, the apparently

quiescent fluid retains a memory of the rotation. This is present in an exact balance of radially-outward centrifugal and radially-inward pressure gradient forces. Perturbing this quiescent state creates an imbalance which expresses itself in a combination of restoring Coriolis and pressure gradient forces that support *inertial waves*. These are the internal waves of a homogeneous-density, rotating fluid. They can be described in a uniformly-rotating Cartesian frame by the constant-coefficient, inviscid rotating linearized Euler equations

$$
\begin{aligned}
u_t - f v &= -p_x, \\
v_t + f u &= -p_y, \\
w_t &= -p_z, \\
\nabla \cdot \mathbf{u} &= 0.
\end{aligned}
\tag{2.19}
$$

Here we use Cartesian velocity vector $\mathbf{u} = (u, v, w)$ and Coriolis parameter, $f = 2\Omega$, again assuming that the vertical z-direction aligns with the rotation axis. The *reduced* pressure p, contains deviations of the true pressure from the combined hydrostatic and cyclostrophic pressure, given by (2.3) and (2.13), respectively. Searching for monochromatic plane-wave solutions, $\propto e^{i(kx+ly+mz-\omega t)}$, with polar representation of wave vector $\mathbf{k} = (k, l, m) = \kappa(\cos\alpha\cos\phi, \cos\alpha\sin\phi, \sin\alpha)$, yields the inertial wave dispersion relation

$$
\omega = \pm 2\Omega \sin\alpha,
\tag{2.20}
$$

which, as for internal gravity waves, is independent of wave vector magnitude κ. Indeed, this equation relates frequency to wave vector inclination relative to the horizontal plane, α, only. This is the hall-mark of internal waves. It complements the frequency—wave number, $\omega(\kappa)$, relationship typical for external waves.

The adjustment of fluids during spin-up or spin-down in basins of non-uniform depth, referred to above, is partly expressed by the inertial waves, described by (2.19). But, in fact, inertial waves arise under adjustment of the rotation rate in any container (Greenspan and Howard 1963; Cederlöf 1988; Oruba et al. 2017), whether forced by viscous or pressure forces. They especially occur when a container is deliberately forced at a frequency less than the Coriolis frequency, for instance by libration—a periodic modulation of the background rotation rate—or, as in nature, by tidal forces, when these waves are sustained (Maas 2001; Manders and Maas 2003, 2004; Bewley et al. 2007; Lamriben et al. 2011; Sibgatullin et al. 2017).

Inertial Waves in an Untilted Box

To solve (2.19) for free inertial waves in a rectangular box that has its sides either perpendicular or parallel to the rotation axis, we use depth H and Coriolis frequency $f = 2\Omega$ as length and inverse time scales (with velocity and reduced pressure scales equaling Hf and $(Hf)^2$, respectively). Note this implies that horizontal dimensions of the box are now measured in terms of H. This leads to the same set (2.19), except that now $f = 1$ and the bottom and surface of the rectangular box are at $z = 0, 1$,

respectively. As the normal velocities at these boundaries vanish, $w(0) = w(1) = 0$, the vertical velocity is expressed as a sum of vertically-standing modes, $w = \sum_{n=1}^{\infty} \partial \zeta_n / \partial t \sin n\pi z$, with ζ_n the vertical displacement field of the nth vertical mode. In turn, this implies $(u, v, p) = \sum_{n=1}^{\infty} (U_n, V_n, P_n) \cos n\pi z$. The vertical momentum equation then yields

$$P_n = \frac{1}{n\pi} \frac{\partial^2 \zeta_n}{\partial t^2}. \tag{2.21}$$

Rescaling the horizontal coordinates $(X, Y) = n\pi(x, y)$, the *same* set of equations describes the horizontal structure of each of the modes, for which reason we suppress mode-index, n. In subscript-derivative notation these read (Maas 2003):

$$\begin{aligned}
U_t - V &= -\zeta_{ttX}, \\
V_t + U &= -\zeta_{ttY}, \\
\zeta_t + U_X + V_Y &= 0.
\end{aligned} \tag{2.22}$$

This set resembles the RSWEs (2.1), except that acceleration of the inertial wave vertical displacement field of mode n,

$$\frac{H}{n\pi} \frac{\partial^2 \zeta_n}{\partial t^2}, \tag{2.23}$$

replaces gravitational acceleration multiplying the free surface displacement, $g\zeta$, which represents the reduced pressure of external, long surface gravity waves, giving due attention to the different meanings of ζ. Each mode obeys the same set of Eqs. (2.22), but finds the box's horizontal size to become larger as n increases. Clearly, as the nth mode scales with the decreasing depth scale, $1/n\pi$, the box's fixed horizontal size, L, increases for this mode to $L_n = n\pi L$.

Inserting plane-monochromatic waves $\propto e^{i(kX+lY-\omega t)}$ into (2.22) yields the dispersion relation

$$\omega^2 = \frac{1}{1 + k^2 + l^2} = \frac{1}{1 + \kappa^2}. \tag{2.24}$$

Its right-hand side is the reciprocal of that for the RSWEs, (2.2). The Coriolis frequency now appears as *high-frequency* instead of low-frequency cut-off. Vertically-standing inertial modes, again behave as external waves, as their frequency now relates to wave vector magnitude of the horizontal wave vector, $\mathbf{k} = (k, l) = \kappa(\cos \phi, \sin \phi)$, like the vertically-standing internal gravity wave modes in a heterogeneous (especially, uniformly-stratified) fluid in a channel or box. As before, however, this apparent external nature of standing internal waves is superficial, owing to the particular orientation of the box, namely with its boundaries perpendicular or parallel to the rotation axis. Before investigating the true nature of inertial waves, which shows up when breaking this symmetry, we should mention how to determine the horizontal structure of inertial waves of this 'untilted' box.
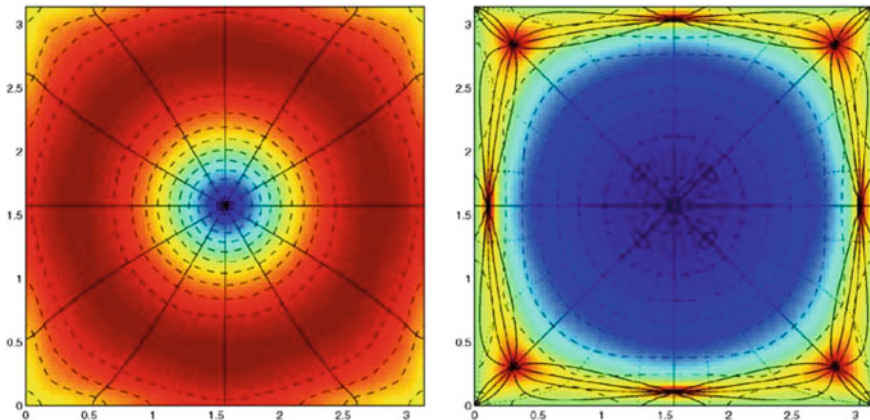
Fig. 2.8 Top view of inertial waves in a cube for the lowest-vertical, lowest-horizontal mode (highest subinertial frequency) of nominal dimensionless frequency $\omega \approx 2^{-1/2}$. Vertical displacement field amplitude (dashed) and phase (solid) (left) and velocity field (right, anticyclonically rotating current vector in blue; cyclonic in red; rectilinear, at walls, in green). For further explanation, see Maas (2003)

Proudman (1916) solved the RSWEs governing the rotationally-modified surface gravity waves in a box by using a Helmholtz decomposition of the horizontal velocity field,

$$\mathbf{u} = -\nabla\phi + \mathbf{e_z} \times \nabla\psi. \tag{2.25}$$

The velocity field is a sum of derivatives of a potential, ϕ, and streamfunction field, ψ. The challenge is to meet impermeability constraints at the box's vertical boundaries. Two-dimensional internal gravity waves need Dirichlet (zero streamfunction) conditions, and three-dimensional internal gravity waves Neumann (zero normal pressure derivative) conditions. Instead, rotationally-modified surface gravity waves require oblique-derivative boundary conditions. In this respect, inertial waves are more complicated than internal gravity waves. The latter execute rectilinear particle motions (within inclined beams), while, in linear approximation, the former follow inclined circular paths. Obviously, in an inviscid description, a side wall can be inserted when it is aligned with the internal gravity wave beam direction. But, circular particle paths, present in an inertial wave beam, are incompatible with any kind of side wall. Clearly, even in the inviscid approach, side walls must give rise to an adjustment of the inertial wave beam's velocity field, suggesting the presence of inviscid, 'wavy' boundary layers.

Proudman's method can also be used to determine the horizontal velocity, (U, V), and vertical displacement, ζ, of the vertically-standing inertial wave field. It leads to a generalized eigenvalue problem, which solves for eigenmodes of decreasing frequency and increasing spatial complexity, see Fig. 2.8. Indeed, as for the RSWEs, amphidromic systems are found (Maas 2003). This includes the fact that each phys-

ical mode (each eigenfrequency) contains an infinite series of Fourier modes, that is, an infinite set of scales, see in particular the corner regions in Fig. 2.8b. The fact that inertial waves are *scale-free* is exploited. The dispersion relation does not constrain the wave number. The interesting difference with rotationally-modified surface gravity waves is that, instead of just a single mode, inertial waves possess an infinite set of vertical modes. This means we might suspect eigenfrequency degeneracy: the eigenfrequency for mode n may be identical to that of another vertical mode m (which perceives the same horizontal domain as being m instead of n times its original horizontal size). The fundamental, beam-like nature of the inertial waves suggests degeneracy. The generalized eigenvalue problem has to be solved numerically. Therefore, a proof that the very same eigenfrequencies will show up for different vertical modes, true for two-dimensional anisotropic as well as for three-dimensional internal gravity waves (Maas 2003), stays a conjecture. In the case of a rotating cube, near-degeneracy is found for waves asymptoting at frequency $1/\sqrt{2}$, but this is no proof of finding the same eigenfrequencies (Wu et al. 2018) .

Inertial Waves in a Tilted Box

Adding an inclined sidewall (Maas 2001), tilting a rectangular box (Ogilvie 2005; Maas 2007), or changing the orientation of boundaries relative to the rotation axis' direction in other ways, implies that, as internal gravity waves, inertial waves will also be subject to focusing and defocusing reflections. In confined, two-dimensional fluid domains this leads to wave focusing dominance. Frequency-dependent orbits again appear to attract waves, regardless where they originate from. Bretherton (1964) inferred that inertial waves approach periodic orbits, giving a geometrical interpretation to prior analytical results by Stern (1963). Stern (1963) described waves in a homogeneous, rotating fluid confined to the equatorial region of a spherical shell, neglecting the vertical acceleration but retaining nontraditional (horizontal) Coriolis terms and noticing the presence of waves decaying polewards, see Maas (2001), Maas and Harlander (2007), Gerkema et al. (2008). Bretherton's (Bretherton 1964) periodic orbit is attracting (Stewartson 1971) and such wave attractors appear to form a broadband phenomenon (Israeli 1972): they exist in continuous frequency bands in which wave attractors have the same topology, experiencing the same amount of reflections at their boundaries. In such frequency windows, attractors have the same *winding number*, the same average angular progression during a single winding around the attractor (Manders et al. 2003). The winding number therefore acts as a topological invariant (Delplace et al. 2017). Instead of fixing the geometry and changing the frequency, this topological property can also be understood from a reverse perspective. Take for example the attractor in the left panel of Fig. 2.7 and keep the frequency, and therefore inclination fixed. Keeping also the attractor's four reflection points at the boundary fixed in space one can otherwise deform the remaining part of the boundary in whatever way one likes, and the attractor will persist as a limit cycle (John 1941). Different boundary deformations lead to differences in convergence rates (measured by the Lyapunov exponent), not in winding number. However, rectangles that are not
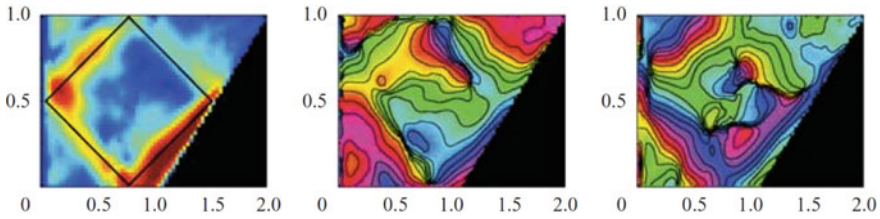
Fig. 2.9 Side view of inertial waves in a trapezoidal basin forced by the libration of a rotating tank. The modulation frequency aims at hitting a square-shaped attractor (solid lines). Visualisation of motions in a vertical sheet, a projection of the three-dimensional currents, is by means of Particle Image Velocimetry. Shown are current amplitude (left) and the phases of the two counter-rotating circular currents (middle and right) into which the current ellipses can be decomposed in the viewing plane. Notice phase lines parallel to attractor branches, indicating transverse phase propagation. For further explanation, see Manders and Maas (2003)

tilted remain exceptional. Ironically these are precisely the geometries favoured in textbooks for being solvable by the method of separation of variables. Lacking the generic appearance of wave attractors, these unfortunately give the completely false suggestion of overall regularity.

The interaction of inertial waves with sloping boundaries was studied experimentally in quasi two-dimensional, Cartesian settings, such as in trapezoidal rectangular basins (Maas 2001; Manders and Maas 2003, 2004; Brunet et al. 2019), see Fig. 2.9, in cylindrical settings such as a conical basin—a frustum—(Klein et al. 2014), and in spherical shells (Koch et al. 2013; Hoff et al. 2016a, b). In all cases, inertial waves, forced by libration of a tank, focus onto 'low-period wave attractors', attractors having the shortest length. Numerical studies, usually of a viscous nature, address the saturation of the amplitude-increase accompanying wave focusing. Saturation, both of focused internal gravity as well as inertial waves, is either due to the appearance of viscous, free boundary layers around the attractor (Rieutord and Valdettaro 1997; Dintrans et al. 1999; Rieutord 2001; Hazewinkel et al. 2008), or to the transfer of energy to other wave frequencies by nonlinear interactions when the fundamental wave experiences Triadic Resonant Instabilities (TRI) (Dauxois et al. 2018).

2.3.3 Three-dimensional Effects

While most studies have concentrated on quasi two-dimensional settings, whether in Cartesian, cylindrical or spherical geometries, inertial waves likely develop three-dimensional fine structure. This is already evident in the horizontal cross-sectional velocity field near the corners of the planar (untilted) box, see Fig. 2.8b. When basin shapes additionally break the reflectional symmetry of the obliquely propagating inertial waves, as in the tilted box or trapezoidal basin, it is a priori clear that wave attractors, located in planes perpendicular to the sloping sides, must adapt to the
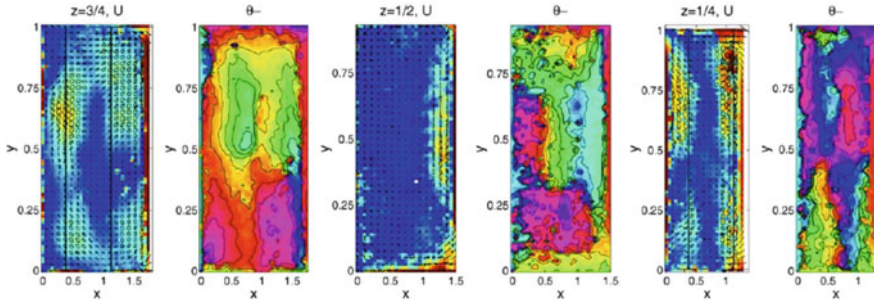
Fig. 2.10 Top view of observed velocity amplitude (U) and anticyclonic phase (θ_-) patterns of inertial waves in a homogeneous fluid contained in a trapezoidal basin. The tank has its sloping side, $z = x - 1$, at the right, for $1 \leq x \leq 2$. Shown are measurements at three heights: ($z = 3/4$, left two panels; $z = 1/2$, middle two panels; $z = 1/4$, right two panels). Inertial waves are forced by libration of the rotating tank. The libration frequency is such that in an infinitely-long trapezoidal basin the inertial wave would approach a rectangular-shaped attractor that intersects these levels at locations indicated by solid black lines. Velocities are dominated by anticyclonic motions. For further explanation, see Manders and Maas (2004)

presence of front and end side-walls. To phrase this differently, while inviscid internal gravity waves in a uniformly-stratified fluid are perfectly able to focus onto a set of wave attractors, all oriented perpendicular to the sloping boundary of a trapezoidal basin, so that their combined structure—the structure of a two-dimensional attracting manifold—is invariant in the along-slope horizontal direction, see Pillet et al. (2018), this is not possible for inertial waves in the same basin. The attracting manifold must change its form, or even its presence, when approaching the front and end walls. An experimental study, aimed at elucidating its structure, found the inertial wave attractor to become more intense but also squeezed on approaching the end walls, see Figs. 2.10 and 2.11. Moreover, wave energy slightly concentrated on the side of the trapezoidal basin that would, from a topographic Rossby wave perspective and given the presence of a sloping bottom, be associated with 'West'.

Other indications for nontrivial behaviour in three-dimensions comes from ray patterns. While rays and characteristics are often considered identical, correct in two-dimensional Cartesian settings, this is not true in three-dimensional or axisymmetric (quasi two-dimensional) domains. For this reason, in contrast to the two-dimensional case of a globally resonant mode, shown in Fig. 2.7b, in a spherical shell globally-resonant modes are not associated with periodicity of all characteristics (Rieutord et al. 2001). Curvature of the boundary implies that in the governing equation the leading second-order operator's characteristics are not identical to energy paths. Yet, this identification works well on small scales where curvature effects are negligible.

The dynamics of internal and inertial wave rays is interesting. The non-specular type of reflection experienced by rays propagating in a plane normal to a sloping bottom or side wall, leading to their focusing or defocusing, also affects the reflection of *obliquely* incident rays. By its elegance, Phillips' derivation of the reflection process of obliquely incident rays, formulated in an *inclined* plane defined by incident
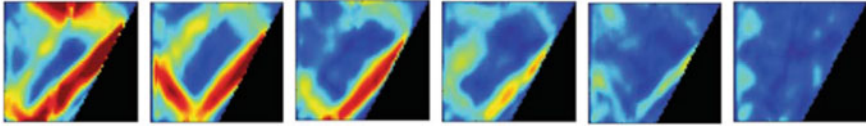
Fig. 2.11 Side views of velocity amplitude (U) measured at six different transects, from left to right at $y/L = 0.12, 0.18, 0.24, 0.30, 0.36, 0.42$ respectively. Notice the elongated character of the attractor close to the side wall at $y = 0$. Picture adapted from Manders and Maas (2003)

and reflected rays (Phillips 1963), obscures somewhat the *instantaneous refraction* accompanying focusing or defocusing reflections: a sudden change in horizontal propagation direction. Describing wave reflection instead in a frame-of-reference whose vertical axis is parallel to the anisotropy direction set by gravity or rotation axis, refraction is seen to occur simultaneously (Maas 2005). Interestingly, in three dimensions focusing of multiply-reflected wave rays onto a wave attractor in a vertical trapping plane is accompanied by another phenomenon that resembles ray behaviour in whispering galleries. Some rays avoid trapping onto a wave attractor by experiencing a sequence of focusing reflections that are exactly balanced by defocusing reflections. Reflection locations hug the line of critical depth, defined as the line connecting depth locations where ray slope equals bottom slope, see Fig. 2.12 (Maas 2005; Rabitti and Maas 2013; Pillet et al. 2019).

2.4   Discussion

The isotropy or anisotropy of a fluid depends on (i) the presence of an anisotropic restoring mechanism, such as gravity, system-rotation, or the presence of a magnetic field, so far undiscussed, (ii) a stratification of the fluid, such as in density or angular momentum, and (iii) the presence of inclined boundaries relative to the anisotropy direction.

The third aspect turns out to be vital. For even when a fluid's density is discretely-stratified in layers, and one might expect interfaces separating the layers to act as horizontal wave guides, see Sect. 2.2.2, or scatter obliquely incident waves into reflected and transmitted oblique waves, experiment shows otherwise (Hazewinkel et al. 2010a). In a fluid having twenty stratified layers of equal depth, differing incrementally in density and confined to a trapezoidal basin, a wave attractor of rectangular shape still forms, see Fig. 2.13. It is very similar in shape to the one found in the uniformly-stratified fluid, as visible in Fig. 2.6. The attractor shape becomes less visible when the number of layers is for instance halved (not shown).

The presence of restoring mechanisms allows us to define equilibrium states, in which a restoring force balances a pressure gradient force, such as the hydrostatic (2.3) and cyclostrophic (2.13) equilibria for density-stratified and rotating,
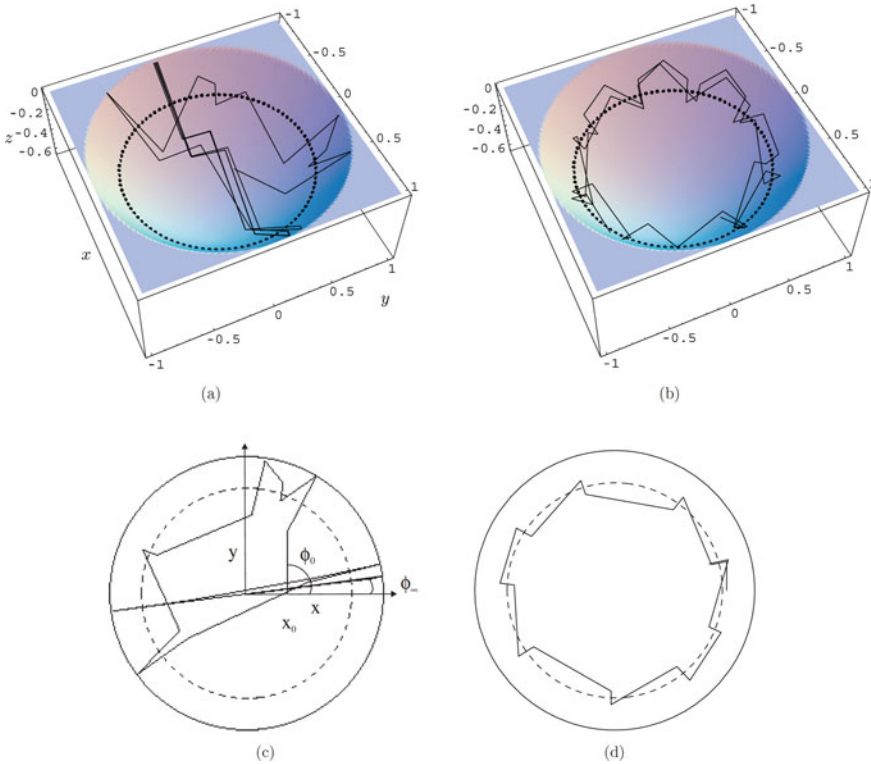
Fig. 2.12 Perspective (**a**, **b**) and top (**c**, **d**) views of rays launched in a uniformly-stratified fluid, confined to a paraboloidal container, either focusing onto a wave attractor (a,c) or propagating around in a whispering-gallery type of motion (b,d). The dashed circles shows critical depths, where bottom slope equals ray slope, determined by the ratio of wave and buoyancy (or Coriolis) frequencies. Picture adapted from Maas (2005)
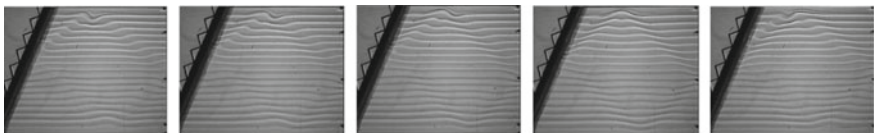

Fig. 2.13 Five subsequent snapshots of a video showing side views of a fluid that is discretely-stratified and that is being oscillated sideways periodically. The fluid contains twenty layers that are incrementally increasing in density downwards. Displacements of interfaces are visualized by shadowgraph. Picture adapted from Hazewinkel et al. (2010a)

homogeneous-density fluids, respectively. In plasmas, the presence of magnetic fields similarly invokes an equilibrium, described by the Grad-Shafranov equations (Goedbloed et al. 2019).

2.4.1 The Linear Shear Flow as 'Problematic' Equilibrium

Notice that waves in shear flows stratified in *linear* momentum, differ from those encountered in fluids stratified in density or angular momentum. Their existence is somewhat of a mystery (Hof et al. 2004). Despite the fact that rectilinear shear flows formally appear as stable solutions of the Euler equations, one cannot pinpoint an equilibrium state consisting in a similar balance of forces that, once disrupted, provides a restoring mechanism. Indeed, regarding the Euler equations as an asymptote of the Navier-Stokes equations in the limit that the Reynolds number $R = UL/\nu \to \infty$ approaches infinity (viscosity $\nu \to 0$), this limiting process, viewed as a state undergoing a large number of bifurcations while increasing the Reynolds number, generates more and more unstable solutions that should necessarily end in turbulence. This relates to the fact that particular classes of waves in shear flows are found in a very circumspect way. This is often done by viewing the rectilinear shear flow either as the limit of a swirling flow inside an annulus, whose cylinders, rotating at different speed, possess radii approaching infinity, or as the limit of a stably-stratified fluid, in which the stratification rate decreases to zero. Conspicuously these exactly correspond to the two previously mentioned cases for which force balances *can* easily be defined. In practice, real viscous pipe flows turn unstable and become turbulent at moderate speeds, generating longitudinal rolls, interacting with subsequently bifurcated transverse circulation cells (Hof et al. 2004). Moreover, because waves that are trapped to a critical layer in a shear flow have a wave frequency depending on wave vector magnitude, these best classify as isotropic again, as the isotropy concept is synonymous with an absence of any wave frequency dependence on wave vector direction.

2.4.2 Waves in Anisotropic Media

By contrast, in anisotropic media wave frequency depends on wave vector direction only, implying that perturbations of hydrostatic and cyclostrophic equilibria are unproblematic. The differences between waves in isotropic and anisotropic media have far-reaching implications. Isotropic water waves, such as surface gravity waves or internal waves in uniform-depth fluids, exhibit focal points when reflecting from convex vertical boundaries (such as a parabolic mirror). However, focusing occurs temporarily. Upon passing a focal point, waves diverge. In confined fluid domains, multiple side-wall reflections of such isotropic waves lead to wave ray chaos. It explains why one can illuminate a cave with a single candle, or why in a popular restaurant, conversations may be lost in a cacophony.

By contrast, anisotropic internal gravity and inertial waves almost always follow an *indefinite* geometric focusing principle. This occurs when they reflect from sloping boundaries that are neither parallel nor perpendicular to the anisotropy direction. As a consequence, despite the fact that linear equations govern these waves, the

geometrically (Maas and Lam 1995) or analytically (Maas 2009) constructed wave solutions exhibit self–similarity in real, Fourier and parameter spaces, features that are normally associated with nonlinear dynamical systems. Also, while isotropic waves in closed basins exhibit a discrete set of eigenfrequencies, the spectrum of anisotropic waves becomes continuous. These and other complementary properties of isotropic and anisotropic waves are discussed in Maas (2005), Brouzet et al. (2017), Sibgatullin and Ermanyuk (2019).

2.4.3 Mixing Due to Wave Focusing and Mean Flows

Let us look at one final aspect of these anisotropic media and their equilibria, namely the impact of waves on the mean state. Perturbations to a balanced hydrodynamic state—waves—may locally provoke mixing. Waves in anisotropic fluids focus onto wave attractors for nearly every shape of the fluid basin. While focusing, along-attractor velocity and shear amplify, and scales reduce. Attractors are therefore locations where mixing of anisotropic fluids can be expected to occur preferentially, either by immediately reaching down to the Kolmogorov scales, where viscous processes can mix, by means of wave breaking due to secondary shear-flow instabilities, or via triadic-wave interactions.

In this manner, local diapycnal (vertical) mixing of a density-stratified fluid leads to horizontal density and pressure gradients that force a horizontal mean flow, so that the mixed fluid will spread out along isopycnal surfaces. As rotating fluids contain a huge amount of energy, stored in rotational motion, weak mechanical forcing can similarly convey part of this large-scale intense flows (Le Bars et al. 2015). But mixing of a homogeneous-density, rotating fluid must pertain to mixing of the 'stuff' the fluid is stratified with: angular momentum. The underlying equilibrium state is thus relevant. The apparently quiescent initial state of a fluid that is in solid-body rotation, i.e. in a frame co-rotating with the container, is radially-stratified in angular momentum. Despite the fact that the (nonlinear) Euler equations are invariant with respect to coordinate translation, they do depend on the rotation axis' *location*. In case the fluid has a free surface this is easily visualised. After the spin-up process, the fluid is in solid-body rotation and the free surface shape will become paraboloidal; to be more precise, a *segment* of a paraboloidal surface. A segment that may or may not contain the paraboloid's minimum, depending on whether or not the rotation axis passes through the container. When that axis lies outside the container, the free surface will have its minimum at the point closest to the rotation axis.

The presence of this paraboloidal surface resolves the chicken-and-egg question whether, away from the rotation axis, the pressure is high because the free surface level is raised in favour of a reversed causality: the free surface is high because the pressure is high. To fully contain the fluid, imagine we use a rigid-lid instead of a free surface. The pressure in this solidly rotating fluid must still increase radially-outward, as fluid continues to be swept outwards by the centrifugal force, and the cyclostrophic balance will persist. While in a rotating, quiescent fluid we can perfectly

well describe perturbations as being governed by the linear, rotating Euler equations, it transpires that, in the same way as we neglect viscous effects after the spin-up phase in these equations, we must also have been neglecting compressibility. Despite liquids being nearly incompressible, during spin-up compressibility must have played a role in setting the higher pressure at larger radii, made visible by the free surface displacement when taking away the rigid lid.

This is relevant to what happens when mixing occurs in a rotating fluid, for instance due to wave focusing. In analogy to the isopycnal spreading of fluid following mixing of density-stratified fluids, mixing of fluids stratified in angular momentum will lead to a mixture spreading out along iso-angular momentum surfaces. But, its subsequent fate depends on the topology of these surfaces relative to the shape and size of the basin. Obviously, axial cylindrical fluid domains—cylinders whose axes coincide with the rotation axis—are special, as all iso-angular momentum surfaces fully lie within the fluid domain. In the presence of a sloping bottom, any mixing triggered by geometric focusing near a wave attractor can then drive a mean flow along a cylindrical iso-angular momentum surface that sits in the container above the attractor's focusing location at the bottom. It is uninhibited by obstructing side walls. Recent experiments on focusing inertial waves confirm the generation of such an axisymmetric mean flow, which however turns unstable and produces a sequence of barotropic cyclones (Boury et al. 2021). But non-axisymmetric boundaries are obviously more generic. When cylindrical iso-angular momentum surfaces are not or not completely contained within the cylinder these lead to regions where iso-angular momentum surfaces are obstructed. This occurs, for instance, in the corners outside the inscribed cylinder of rectangular axial containers. More pathologically this occurs for basins that lie completely outside the rotation axis, as for instance an eccentrically-positioned container on a large turn-table (Maas 2001). In that case, *all* angular momentum surfaces intersect the boundary and closed angular momentum surfaces are completely absent, see Fig. 2.14.

The notion of iso-angular momentum surfaces, and their potential blockage by boundaries, is reminiscent of that of geostrophic contours (Rhines and Young 1982). The latter are lines of equal potential vorticity, f/h, the ratio of planetary vorticity f and fluid depth, h. In geophysical context these lines are typically oriented in zonal direction because in the traditional approximation only the vertical component of planetary vorticity is taken into account. Variations in bottom topography, or, in a two-layer context, in equivalent depth, related to the interface depth, can force these lines to develop closed contours. Within these contours, circulation can strongly amplify and homogenise potential vorticity. We anticipate that the presence of closed iso-angular momentum surfaces may similarly homogenise angular momentum, even in uniform-depth, rigid-lid containers where potential vorticity is constant.
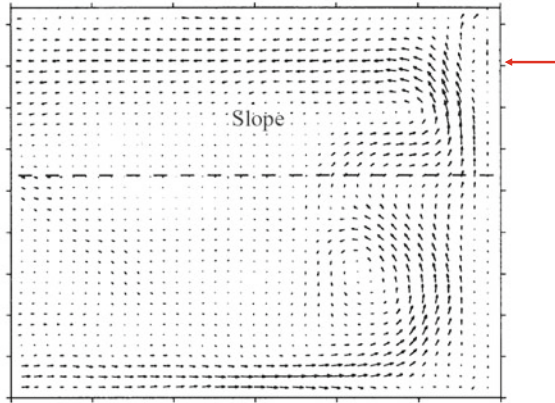
Fig. 2.14 Eulerian, vertically-uniform mean-flow observed by means of PIV in the top view of a homogeneous-density, rotating fluid situated in an eccentrically-located tank that is subject to libration. Observations extend over the right-half of the tank only. The angular momentum surfaces are roughly aligned with the figure's lower boundary. An attractor manifold develops (far from the vertical wall, at the right) over the location where it reflects from the slope, indicated by the red arrow. At the attractor, fluid differing in angular momentum is mixed, forcing this mean-flow. Picture adapted from Maas (2001)

2.5   Conclusion

A fluid layer supports waves that find their maxima and minima either at its boundaries or in its interior: external and internal waves, respectively. The former class encompasses capillary and surface and interfacial gravity waves, found in isotropic media. They obey a dispersion relation that relates frequency to wave vector magnitude. The latter class, encompassing internal gravity and inertial waves are found in anisotropic media. By contrast, their dispersion relations relate frequency to wave vector direction. The consequences of this difference in dispersion relation are multiple, best summarised by stating that the behaviour of internal waves is completely opposite and complementary to that of external waves.

In a field of gravity, anisotropy can be due to a stratification (non-uniformity) of the fluid's density. In a rotating fluid, anisotropy may be due to a radial stratification in angular momentum. These stratifications lend fluid parcels 'a memory', expressed in the material conservation of their density or angular momentum, respectively. Quiescent fluids that are stably stratified in density or angular momentum possess a balance between two opposing forces. Perturbing these states gives rise to a restoring mechanism, as one of the two forces will dominate.

Shear flows represent fluids that are stratified in linear momentum. With the exception of linear or parabolic shear flows, as present in Couette and Poiseuille flows, respectively, these flows do not themselves obey the Navier-Stokes equations. Under some stability conditions, these flows also support waves but lack an underlying balance of forces, making it harder to identify an internal restoring mechanism.

References

Berry, M.V. 1981. Regularity and chaos in classical mechanics, illustrated by three deformations of a circular 'billiard'. *European Journal of Physics* 2: 91.

Bewley, G.P., D.P. Lathrop, L.R.M. Maas, and K.R. Sreenivasan. 2007. Inertial waves in rotating grid turbulence. *Physics of Fluids* 19 (7): 071701.

Boury, S., I. Sibgatullin, E. Ermanyuk, N. Shmakova, P. Odier, S. Joubaud, L.R.M. Maas and T. Dauxois. 2021. Vortex cluster arising from an axisymmetric inertial wave attractor. *Journal of Fluid Mechanics*, 926 (A12).

Bretherton, F.P. 1964. Low frequency oscillations trapped near the equator. *Tellus* 16 (2): 181–185.

Brouzet, C., I.N. Sibgatullin, E.V. Ermanyuk, S. Joubaud, and T. Dauxois. 2007. Scale effects in internal wave attractors. *Physical Review Fluids* 2 (11): 114803.

Brunet, M., T. Dauxois, and P.-P. Cortet. 2019. Linear and nonlinear regimes of an inertial wave attractor. *Physical Review Fluids* 4 (3): 034801.

Burnside, W. 1888. On the small wave-motions of a heterogeneous fluid under gravity. *Proceedings of the London Mathematical Society* 1 (1): 392–397.

Carpenter, J.R., E.W. Tedford, E. Heifetz, and G.A. Lawrence. 2011. Instability in stratified shear flow: Review of a physical interpretation based on interacting waves. *Applied Mechanics Reviews* 64 (6): 060801.

Cederlöf, U. 1988. Free-surface effects on spin-up. *Journal of Fluid Mechanics* 187: 395–407.

Darrigol, O. 2005. *Worlds of flow: A history of hydrodynamics from the Bernoullis to Prandtl.* Oxford University Press.

Dauxois, T., S. Joubaud, P. Odier, and A. Venaille. 2018. Instabilities of internal gravity wave beams. *Annual Review of Fluid Mechanics* 50: 131–156.

Delplace, P., J.B. Marston, and A. Venaille. 2017. Topological origin of equatorial waves. *Science* 358 (6366): 1075–1077.

Dintrans, B., M. Rieutord, and L. Valdettaro. 1999. Gravito-inertial waves in a rotating stratified sphere or spherical shell. *Journal of Fluid Mechanics* 398: 271–297.

Drazin, P.G., and L.N. Howard. 1962. The instability to long waves of unbounded parallel inviscid flow. *Journal of Fluid Mechanics* 14 (2): 257–283.

Drazin, P.G., and W.H. Reid. 1998. *Hydrodynamic stability.* Cambridge University Press.

Ekman, V.W. 1904. On dead water. *Norwegian North Polar expedition 1893–1896, scientific results*, 5 (15): 1–152.

Fjeldstad, J.E. 1933. *Interne wellen. Geofysiske Publikasjoner* 10 (6): 1–35.

Franklin, B. 1762. Relating a curious instance of the effect of oil on water. *Complete Works, London* 2: 142, 1762.

Gerkema, T., J.T.F. Zimmerman, L.R.M. Maas, and H. Van Haren. 2008. Geophysical and astrophysical fluid dynamics beyond the traditional approximation. *Reviews of Geophysics* 46(2).

Gill, A.E. 1982. *Atmosphere-ocean dynamics.* Ac Press.

Goedbloed, H., R. Keppens, and S. Poedts. 2019. *Magnetohydrodynamics of laboratory and astrophysical plasmas.* Cambridge University press.

Greenspan, H.P., and L.N. Howard. 1963. On a time-dependent motion of a rotating fluid. *Journal of Fluid Mechanics* 17 (3): 385–404.

Grimshaw, R., E. Pelinovsky, and T. Talipova. 2010. Nonreflecting internal wave beam propagation in the deep ocean. *Journal of Physical Oceanography* 40 (4): 802–813.

Groen, P. 1948. *Contribution to the theory of internal waves.* KNMI, Mededelingen en verhandelingen; Serie B, Deel II, No. I.

Hazewinkel, J., P. van Breevoort, S.B. Dalziel, and L.R.M. Maas. 2008. Observations on the wavenumber spectrum and evolution of an internal wave attractor. *Journal of Fluid Mechanics* 598: 373–382.

Hazewinkel, J., L.R.M. Maas & S.B. Dalziel (2010a). Attractive internal wave patterns. arXiv:1010.1046 [physics.flu-dyn].

Hazewinkel, J., Chr. Tsimitri, L.R.M. Maas, and S.B. Dalziel. 2010. Observations on the robustness of internal wave attractors to perturbations. *Physics of Fluids* 22 (10): 107102.

Heller, E.J. 1984. Bound-state eigenfunctions of classically chaotic Hamiltonian systems: Scars of periodic orbits. *Physical Review Letters* 53 (16): 1515–1518.

Hinwood, J.B. 1972. The study of density-stratified flows up to 1945 part 2 internal waves and interfacial effects. *La Houille Blanche* 8 (709–722): 1972.

Hof, B., C.W.H. van Doorne, J. Westerweel, F.T.M. Nieuwstadt, H. Faisst, B. Eckhardt, H. Wedin, R.R. Kerswell, and F. Waleffe. 2004. Experimental observation of nonlinear traveling waves in turbulent pipe flow. *Science* 305 (5690): 1594–1598.

Hoff, M., U. Harlander, and C. Egbers. 2016. Experimental survey of linear and nonlinear inertial waves and wave instabilities in a spherical shell. *Journal of Fluid Mechanics* 789: 589–616.

Hoff, M., U. Harlander, and S.A. Triana. 2016. Study of turbulence and interacting inertial modes in a differentially rotating spherical shell experiment. *Physical Review Fluids* 1 (4): 043701.

Israeli, M. 1972. On trapped modes of rotating fluids in spherical shells. *Studies in Applied Mathematics* 51 (3): 219–237.

John, F. 1941. The dirichlet problem for a hyperbolic equation. *American Journal of Mathematics* 63 (1): 141–154.

Kelvin, Lord. 1880. On the oscillations of a columnar vortex. *Philosophical Magazine* 10: 155–168.

Klein, M., T. Seelig, M.V. Kurgansky, A. Ghasemi, I.D. Borcia, A. Will, E. Schaller, Chr. Egbers, and U. Harlander. 2014. Inertial wave excitation and focusing in a liquid bounded by a frustum and a cylinder. *Journal of Fluid Mechanics* 751: 255–297.

Koch, S., U. Harlander, Chr. Egbers, and R. Hollerbach. 2013. Inertial waves in a spherical shell induced by librations of the inner sphere: experimental and numerical results. *Fluid Dynamics Research* 45 (3): 035504.

Krauss, W. 1973. *Dynamics of the homogeneous and the quasihomogeneous ocean*, vol. 1. Borntraeger.

Lamriben, C., P.-P. Cortet, F. Moisy, and L.R.M. Maas. 2011. Excitation of inertial modes in a closed grid turbulence experiment under rotation. *Physics of Fluids* 23 (1): 015102.

Le Bars, M., D. Cébron, and P. Le Gal. 2015. Flows driven by libration, precession, and tides. *Annual Review of Fluid Mechanics* 47: 163–193.

Li, L., M.D. Patterson, K. Zhang, and R.R. Kerswell. 2012. Spin-up and spin-down in a half cone: A pathological situation or not? *Physics of Fluids* 24 (11): 116601.

Love, A.E.H. 1890. Wave-motion in a heterogeneous heavy fluid. *Proceedings of the London Mathematical Society* 1 (1): 307–316.

Maas, L.R.M. 2001. Wave focusing and ensuing mean flow due to symmetry breaking in rotating fluids. *Journal of Fluid Mechanics* 437: 13–28.

Maas, L.R.M. 2003. On the amphidromic structure of inertial waves in a rectangular parallelepiped. *Fluid Dynamics Research* 33 (4): 373–401.

Maas, L.M.R. 2005. Wave attractors: Linear yet nonlinear. *International Journal of Bifurcation and Chaos in Applied Sciences and Engineering* 15(9): 2757–2782.

Maas, L.R.M. 2007. Experiments on rotating flows: Impact of rotation on flow through tilted rectangular ducts. In *St. Petersburg Conference "Fluxes and Structures in Fluids"*, Ed. Yu. Chashechkin, 1–10.

Maas, L.R.M. 2009. Exact analytic self-similar solution of a wave attractor field. *Physica D* 238 (5): 502–505.

Maas, L.R.M., and U. Harlander. 2007. Equatorial wave attractors and inertial oscillations. *Journal of Fluid Mechanics* 570: 47–67.

Maas, L.R.M., and F.P.A. Lam. 1995. Geometric focusing of internal waves. *Journal of Fluid Mechanics* 300: 1–41.

Manders, A.M.M., and L.R.M. Maas. 2003. Observations of inertial waves in a rectangular basin with one sloping boundary. *Journal of Fluid Mechanics* 493: 59–88.

Manders, A.M.M., and L.R.M. Maas. 2004. On the three-dimensional structure of the inertial wave field in a rectangular basin with one sloping boundary. *Fluid Dynamics Research* 35 (1): 1–21.

Manders, A.M.M., J.J. Duistermaat, and L.R.M. Maas. 2003. Wave attractors in a smooth convex enclosed geometry. *Physica D* 186 (3–4): 109–132.

Nansen, F. 1902. The oceanography of the north polar basin. *The Norwegian North Polar Expedition 1893–1896. Scientific Results* 3(9).

Ogilvie, G.I. 2005. Wave attractors and the asymptotic dissipation rate of tidal disturbances. *Journal of Fluid Mechanics* 543: 19–44.

Oruba, L., A.M. Soward, and E. Dormy. 2017. Spin-down in a rapidly rotating cylinder container with mixed rigid and stress-free boundary conditions. *Journal of Fluid Mechanics* 818: 205–240.

Phillips, O.M. 1963. Energy transfer in rotating fluids by reflection of inertial waves. *Physics of Fluids* 6 (4): 513–520.

Pillet, G., E.V. Ermanyuk, L.R.M. Maas, I.N. Sibgatullin, and T. Dauxois. 2018. Internal wave attractors in three-dimensional geometries: Trapping by oblique reflection. *Journal of Fluid Mechanics* 845: 203–225.

Pillet, G., L.R.M. Maas, and T. Dauxois. 2019. Internal wave attractors in 3d geometries: A dynamical systems approach. *European Journal of Mechanics - B/Fluids* 77: 1–16.

Proudman, J. 1916. On the dynamical theory of tides. Part II. Flat seas. *Proceedings of the London Mathematical Society, 2nd Series* 18: 21–50.

Rabitti, A., and L.R.M. Maas. 2013. Meridional trapping and zonal propagation of inertial waves in a rotating fluid shell. *Journal of Fluid Mechanics* 729: 445–470.

Rao, D.B. 1966. Free gravitational oscillations in rotating rectangular basins. *Journal of Fluid Mechanics* 25 (03): 523–555.

Rayleigh, Lord. 1879. On the stability, or instability, of certain fluid motions. *Proceedings of the London Mathematical Society* 1 (1): 57–72.

Rayleigh, Lord. 1883. Investigation of the character of the equilibrium of an incompressible heavy fluid of variable density. *Proceedings of the London Mathematical Society* 14: 170–177.

Rayleigh, Lord. 1917. On the dynamics of revolving fluids. *Proceedings of the Royal Society A* 93 (648): 148–154.

Rhines, P.B., and W.R. Young. 1982. Homogenization of potential vorticity in planetary gyres. *Journal of Fluid Mechanics* 122: 347–367.

Rieutord, M. 2001. Ekman layers and the damping of inertial r-modes in a spherical shell: application to neutron stars. *Astrophysical Journal* 550 (1): 443–447.

Rieutord, M., and L. Valdettaro. 1997. Inertial waves in a rotating spherical shell. *Journal of Fluid Mechanics* 341: 77–99.

Rieutord, M., B. Georgeot, and L. Valdettaro. 2001. Inertial waves in a rotating spherical shell: Attractors and asymptotic spectrum. *Journal of Fluid Mechanics* 435: 103–144.

Sibgatullin, I.N., and E.V. Ermanyuk. 2019. Internal and inertial wave attractors: A review. *Journal of Applied Mechanics and Technical Physics* 60 (2): 284–302.

Sibgatullin, I.N., E. Ermanyuk, L.R.M. Maas, X. Xu, and T. Dauxois. 2017. Direct numerical simulation of three-dimensional inertial wave attractors. In *2017 Ivannikov ISPRAS Open Conference (ISPRAS)*, pp 137–143.

Squire, H.B. 1933. On the stability for three-dimensional disturbances of viscous fluid flow between parallel walls. *Proceedings of the Royal Society A* 142 (847): 621–628.

Steinmoeller, D.T., M. Stastna, and K.G. Lamb. 2019. Calculating basin-scale free oscillations in lakes on a rotating earth. *Ocean Modelling* 139: 101403.

Stern, M.E. 1963. Trapping of low frequency oscillations in an equatorial "boundary layer". *Tellus* 15 (3): 246–250.

Stewartson, K. 1971. On trapped oscillations of a rotating fluid in a thin spherical shell. *Tellus* 23 (6): 506–510.

Stokes, G.G. 1847. On the theory of oscillatory waves. *Transactions of the Cambridge Philosophical Society* 8: 441.

Sun, J., C.J. Nappo, L. Mahrt, D. Belušić, B. Grisogono, D.R. Stauffer, M. Pulido, C. Staquet, Q. Jiang, A. Pouquet, et al. 2015. Review of wave-turbulence interactions in the stable atmospheric boundary layer. *Reviews of Geophysics* 53 (3): 956–993.

Sverdrup, H.U. 1926. Dynamics of tides on the northern Siberian shelf. *Geophysics Publication* 4 (5): 76.

Taylor, G.I. 1922. Tidal oscillations in gulfs and rectangular basins. *Proceedings of the London Mathematical Society* 2 (1): 148.

Van Heijst, G.J.F. 1989. Spin-up phenomena in non-axisymmetric containers. *Journal of Fluid Mechanics* 206: 171–191.

Van Heijst, G.J.F., P.A. Davies, and R.G. Davis. 1990. Spin-up in a rectangular container. *Physics of Fluids* 2 (2): 150–159.

Van Heijst, G.J.F., L.R.M. Maas, and C.W.M. Williams. 1994. The spin-up of fluid in a rectangular container with sloping bottom. *Journal of Fluid Mechanics* 265: 125–159.

Vogt, T., D. Räbiger, and S. Eckert. 2014. Inertial wave dynamics in a rotating liquid metal. *Journal of Fluid Mechanics* 753: 472–498.

Waleffe, F. 1997. On a self-sustaining process in shear flows. *Physics of Fluids* 9 (4): 883–900.

Weidman, P.D. 1976. On the spin-up and spin-down of a rotating fluid. part 1. extending the Wedemeyer model. *Journal of Fluid Mechanics* 77(4): 685–708.

Whewell, W. 1833. Essay towards a first approximation to a map of cotidal lines. *Philosophical Transactions of the Royal Society of London* 147–236.

Wu, K., B.D. Welfert, and J.M. Lopez. 2018. Complex dynamics in a stratified lid-driven square cavity flow. *Journal of Fluid Mechanics* 855: 43–66.